

# (Sub)mm continuum observations of NGC 6334A

Göran Sandell

National Radio Astronomy Observatory\*, P.O. Box 2, Green Bank, WV 24944, USA

Received 30 October 1998 / Accepted 9 December 1998

**Abstract.** We present 2 mm, 1.1 mm, 850  $\mu\text{m}$ , 800  $\mu\text{m}$ , and 450  $\mu\text{m}$  mapping and photometry of the field surrounding NGC 6334A. We find a prominent east–west dust ridge, approximately centered on NGC 6334A. We interpret this ridge as a collimating dust disk or torus and derive a mass of  $\sim 60 M_{\odot}$  from our continuum data. It is possible though, that this disk–like structure is contaminated on the west-side by a protostellar source, seen as an  $\text{H}_2\text{O}$  maser. We find a second strong source MM2, near MM1 in the immediate vicinity of the HII region.  $\text{H}^{13}\text{CO}^+$   $J = 4-3$  spectra of MM1 and MM2 confirm that it is a separate source. MM2 approximately coincides with IRS3, a 10  $\mu\text{m}$  source, which in earlier studies has been proposed to be a protostar. We estimate MM2/IRS3 to have a mass of  $\sim 50 M_{\odot}$ . We find two other protostellar candidates: MM3 and MM4. MM3 is a relatively compact source with a mass of  $150 M_{\odot}$  and connected by a ridge of dust to the HII region, while MM4 is fainter and more extended.

We also see a thin shell of dust surrounding the red–shifted ionized outflow lobe, presumably swept up by the outflow. The dust shell has a mass of  $\sim 60 M_{\odot}$ . There is clearly less dust emission towards the north, and we do not see the same interaction between the ionized outflow and the surrounding molecular cloud as we see to the south.

**Key words:** ISM: dust, extinction – ISM: H II regions – ISM: individual objects: NGC 6334A – ISM: jets and outflows – radio continuum: ISM – submillimeter

## 1. Introduction

It is now rather well established that many young stellar objects (YSOs) drive energetic outflows, although the mechanism by which these outflows are driven is not yet fully understood. Most outflows are observed in molecular lines like CO and appear bipolar with various degree of collimation. Some outflows are also associated with fast optical jets (see e.g. Mundt et al. 1987), while some also show up in atomic or ionized gas (Lizano et al. 1988, Rodríguez et al. 1994), although it is generally argued

that an ionized wind carries insufficient momentum to drive molecular outflows.

A rather recent discovery, however, is bipolar outflows in ionized gas surrounding ultracompact HII (UCHII) regions (de Pree et al. 1993, 1994). De Pree et al. used the VLA to image the well studied UCHII region K3–50 in  $\text{H}76\alpha$  and found that the ionized emission is blue–shifted on one side and red–shifted on the other, i.e. similar to the more common phenomenon of molecular bipolar outflows.

Before the work of de Pree et al. (1993, 1994), Rodríguez, Cantó, & Moran (1988) reported observations of NGC 6334A, which showed ionized lobes surrounding the HII region, forming a seemingly bipolar structure. They interpreted the lobes as being ionized by NGC 6334A through holes in the shell surrounding the ionizing star. They also suggested that the bipolar morphology may be collimated by a flattened disk or torus surrounding the HII region, since FIR observations by Harvey & Gatley (1984) show an east–west ridge approximately centered on NGC 6334A. They predicted that the northern lobe should be tilted towards us (blue–shifted), since the northern lobe appears less obscured. Recent observations in  $\text{H}92\alpha$  by De Pree et al. (1995) confirm that the bipolar lobes seen emanating from the star are due to an outflow of ionized gas, with the southern lobe being red–shifted relative to the northern one.

Observations in the sub–mm provide far higher angular resolution than can currently be obtained in the FIR. We therefore decided to use sub–mm photometry and mapping to look whether there is a dust–disk surrounding NGC 6334A and whether there are other sources in the vicinity, which may contribute to the total luminosity. Below we present calibrated maps at 2.0, 1.1 mm, and 800  $\mu\text{m}$  as well as uncalibrated SCUBA images at 850 and 450  $\mu\text{m}$  and discuss the implications derived from these observations.

## 2. Observations and data reduction

Most observations were taken with the common user bolometer UKT14 on the 15m James Clerk Maxwell Telescope<sup>1</sup>, on Mauna

---

Send offprint requests to: G. Sandell (gsandell@nrao.edu)

\* The National Radio Astronomy Observatory is a facility of the National Science Foundation operated under cooperative agreement by Associated Universities, Inc.

---

<sup>1</sup> The James Clerk Maxwell Telescope is operated on a joint basis between the United Kingdom Particle Physics and Astronomy Research Council (PPARC), the Netherlands Organisation for the Advancement of Pure Research (ZWO), the Canadian National Research Council (NRC), and the University of Hawaii (UH).

Kea, Hawaii, during one observing run in March 1991. We have also added two uncalibrated SCUBA images taken in October 1996, because even though the maps are not calibrated, the 850 and 450  $\mu\text{m}$  maps go rather deep and especially the 450  $\mu\text{m}$ -map provides better resolution than the UKT14 maps, although over a more limited field.

UKT14 is a sensitive,  $^3\text{He}$ -cooled, one channel bolometer with a filter wheel and a variable iris that permits diffraction limited observations from 1.1 mm – 350  $\mu\text{m}$ . For longer wavelengths the optics over-illuminate the primary. The instrument is described in more detail by Duncan et al. (1990). Details of photometry observing techniques and reduction are also presented by Sandell (1994).

SCUBA is the new common user bolometer array for JCMT, with 37 long wavelength bolometers and 91 short-wavelength ones. Both arrays can be used simultaneously. For a recent description of SCUBA, see e.g. Holland et al. (1998).

The weather conditions were rather marginal during the UKT14 observations, with 2–5 mm of precipitable water vapor, permitting observations only down to 800  $\mu\text{m}$ . Calibration was derived from observations of Uranus, and the secondary calibrators 16293-2422, G5.89, and NGC 6334I (Sandell 1994), the latter being rather close to NGC 6334A. Continuum maps in on-the-fly mode, i.e. continuously scanning in Azimuth while chopping in the scan direction, were obtained at 2 mm, 1.1 mm, and 800  $\mu\text{m}$ . For 2 mm we sampled every 9", at 1.1 mm every 5", while the 800  $\mu\text{m}$ -map was obtained with a 4" sampling. At 2 mm we obtained two relatively small maps, at 1.1 mm a total of three, but at 800  $\mu\text{m}$  we were only able to secure one map. The 800  $\mu\text{m}$ -map was taken in rather marginal weather conditions and shows some evidence of striping in the scan direction, but otherwise it looks remarkably similar to the 1.1 mm map. The pointing was checked before and after each map using NGC 6334I as a reference; pointing drifts (typically 3–4") during the map were removed in the data reduction. However, the submillimeter position of NGC 6334I is somewhat uncertain, and we estimate our positional accuracy to be  $\sim 3''$ . All maps were reduced using both the NOD2 software package (Haslam 1974) and the maximum entropy reconstruction algorithm DBMEM (Richer 1992). The DBMEM images were recalibrated using the integrated fluxes deduced from the calibrated NOD2 maps assuming an error lobe contribution of 10% at 1.1 mm and 20% at 800  $\mu\text{m}$ . Note that since the 1.1mm map is a coadd of three maps, all with different spatial coverage, the noise level is not uniform over the map. The north-eastern portion of the 1.1 mm map is only covered by one map taken in rather marginal sky conditions, and has a noise level about twice that of the best map. We have smoothed the 1.1 mm and 800  $\mu\text{m}$ -maps with an arbitrary 6" beam (which does not mean that we achieve a 6"-resolution) to allow direct comparison between the 1.1 mm and 800  $\mu\text{m}$  maps, which are presented in Fig. 1.

The SCUBA observations were done as jiggle maps in excellent submillimeter conditions. The chop throw was 120" in Azimuth. There is some indications that we chopped on some extended dust emission outside our field of view, but this is not

**Table 1.** Continuum photometry of NGC 6334A. All fluxes are given in Jy/beam

Filter/HPBW	Flux	
	[Jy/beam]	(N)
2.0mm/27"	7.98 $\pm$ 0.27	(3)
1.3mm/19.5"	8.51 $\pm$ 0.11	(2)
1.1mm/18.5"	10.16 $\pm$ 0.03	(2)
800 $\mu\text{m}$ /16.5"	24.4 $\pm$ 0.3	(2)

**Table 2.** Source positions deduced from the 1.1 mm and 800  $\mu\text{m}$  continuum maps and sizes from the 450  $\mu\text{m}$ -map. Since MM1a,b and MM2 all appear extended and are partially overlapping, especially at the longer wavelengths, the measured source sizes are expected to be overestimates.

SOURCE	$\alpha \times \delta$	p.a.	R.A.	DEC.
	(")	°	(1950) h m s	(1950) ° ' "
MM1a	25 $\times$ 9	–66	17 16 58.2	– 35 51 42.5
MM1b	20 $\times$ 10	+68	17 16 57.2	– 35 51 45.0
MM2	16 $\times$ 12	–67	17 16 56.9	– 35 52 00.0
MM3	14 $\times$ 11	–78	17 17 02.8	– 35 51 59.0
MM4	37 $\times$ 14	20	17 17 00.9	– 35 52 44.0

likely to affect the morphology of the dust emission, except perhaps in north west. The SCUBA images are show in Fig. 2.

To test whether there is a velocity gradient over the dust ridge on NGC 6334A, we obtained a few spectra in  $\text{H}^{13}\text{CO}^+ \text{J} = 4-3$ , which is expected to trace optically thin gas. These observations were done on December 26, 1994 with RxB3i, our common user 300 GHz receiver. At 347 GHz the HPBW is  $\sim 14.5''$ , which does not allow us to resolve the disk-like structure seen toward the HII region. Spectra were obtained on A, MM1a, MM1b and MM2. The systemic velocity of NGC 6334A is  $V_{lsr} = -3.3 \text{ km s}^{-1}$ .

### 3. Results

#### 3.1. Morphology

The 1.1 mm map (Fig. 1a), which has the largest spatial coverage, gives a good overview of the dust emission associated with the NGC 6334A complex. In Table 1 we give positions of sources, which are seen both in the 1.1 mm and 800  $\mu\text{m}$  maps as well as in the SCUBA maps, and which have positional agreement  $\leq 2''$ .

Strong dust emission is seen towards NGC 6334A. At high resolution this emission resolves into three sources: MM1a, MM1b, and MM2 (Fig. 2). MM1 is a double peaked source, approximately centered on the HII region. It is not clear, whether this is a single source or two separate sources. MM1a is clearly associated with the torus that we suggest surrounds the HII region, while MM1b, especially in the 450  $\mu\text{m}$ -map shifts more to the west and appears like a much more compact source, possible associated with the  $\text{H}_2\text{O}$  maser just outside the HII

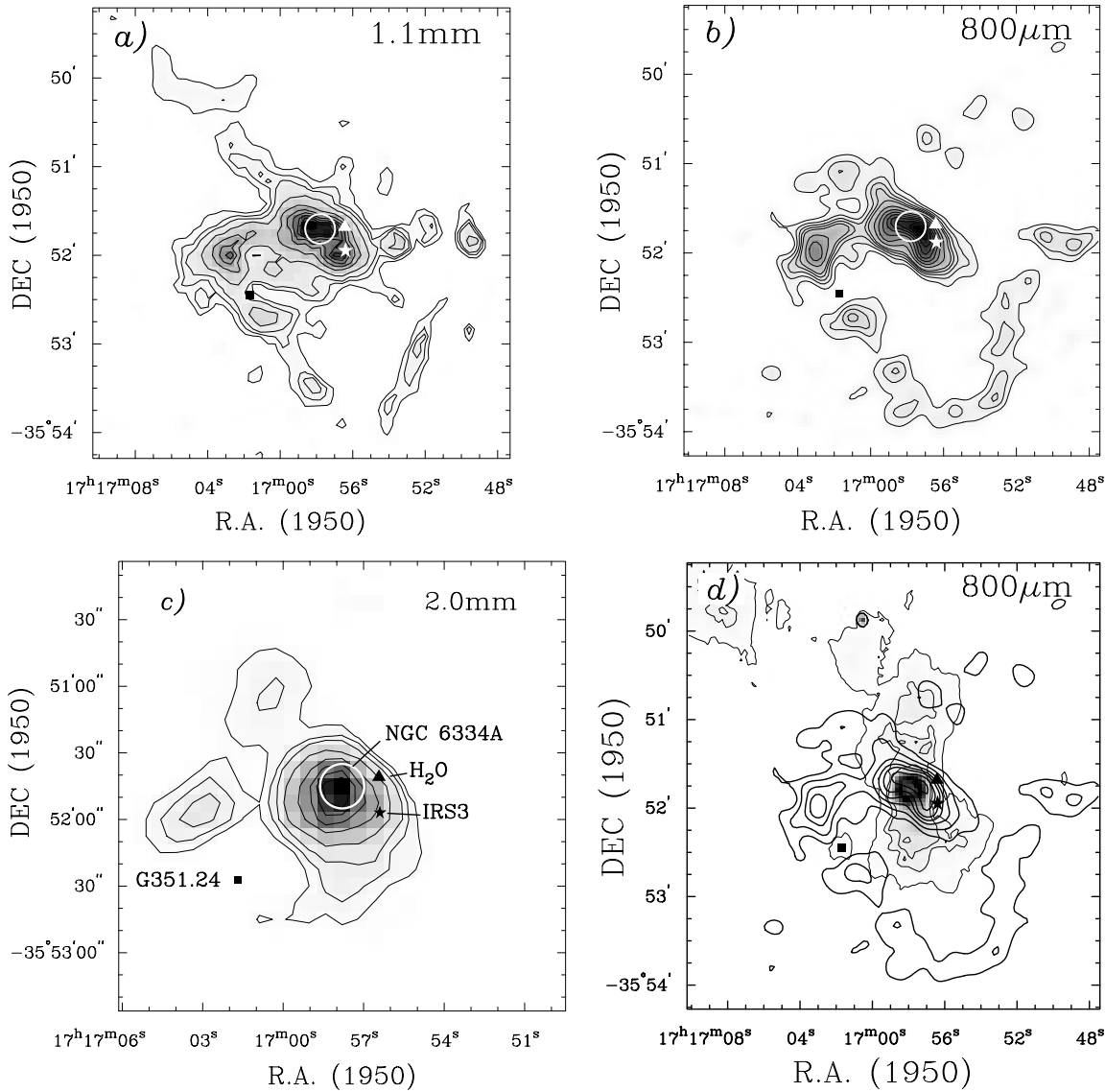


**Fig. 1.** **a** Greyscale plot overlaid with contours of the 1.1 mm emission surrounding NGC 6334A. The position of the HII region A is marked by a circle. The position of the H<sub>2</sub>O maser is marked by a filled triangle, the 10 μm protostellar source by a star, and the second HII region by a square, as labelled in **c**. **b** Same as in **a** but for 800 μm. Note that the 800 μm map does not cover the same area as the 1.1 mm map. There are no data from ~50'' north-east of A. **c** The more limited field mapped at 2 mm. **d** The same 800 μm map as shown in **b**, but shown with contours only, and overlaid with the free-free emission mapped by Rodríguez, Cantó, & Moran (1988). The free-free emission is plotted with thinner contours than the dust emission and enhanced with a grey scale.

region. H<sup>13</sup>CO<sup>+</sup> J = 4–3 spectra towards towards A, MM1a and MM1b all have about the same radial velocity, i.e.  $V_{lSR} = -3.3$  km s<sup>-1</sup>, while a spectrum taken towards MM2 has a  $V_{lSR} = -4.5$  km s<sup>-1</sup>, a velocity shift of more than 1 km s<sup>-1</sup> from that of the HII region (Fig. 3). MM2 is clearly outside the HII shell and kinematically separate from MM1. It is ~6'' from the 10 μm source IRS 3, which is almost certainly associated with MM2. Another strong extended bow-shaped source (MM3) is located ~60'' east of the HII region and connecting to it by a bridge of emission. There is also some faint lumpy emission on the west side extending ~100'' from the HII region. MM3, the eastern source, also connects to the south-west into another

fainter source, MM4, although there is a gap roughly half way in between, where there is another faint HII region, G351.54+0.65 (De Pree et al. 1995), which appears to have freed itself from dust completely. This HHII-region is faintly seen even in the map by Rodríguez, Cantó, & Moran (1988), c.f. overlay in Fig. 1d. From MM4 the dust emission continues into a loop of faint emission extending ~100'' south of A. There is also an extended ridge to the north-east. The 800 μm-map (Fig. 1b), which has more limited coverage to the north, only shows the beginning of the ridge, but otherwise the 1.1 mm and 800 μm-maps are remarkably similar. One can clearly see the strong emission associated with A, but not as clearly double peaked as in the 1.1 mm-map.

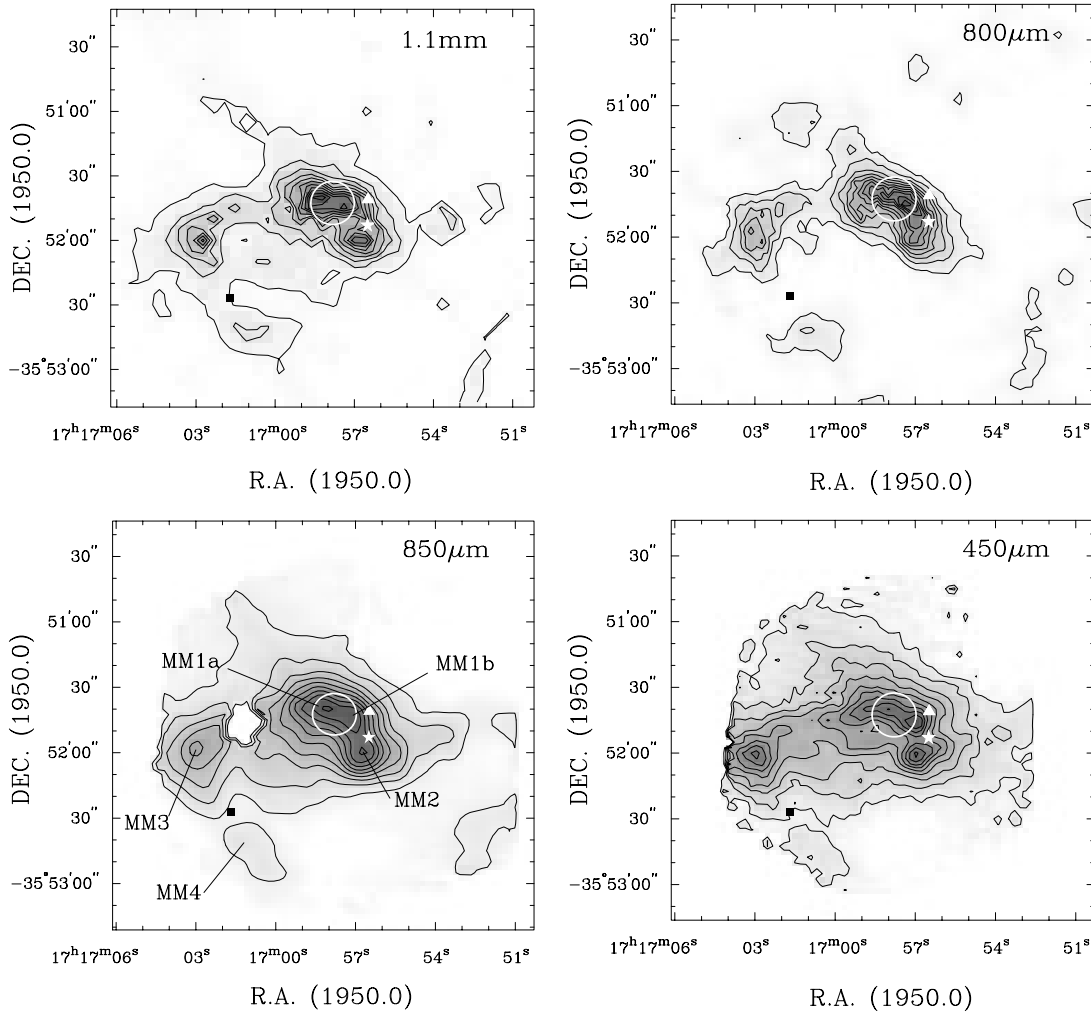


**Fig. 2.** Contour plots with greyscale of the central area surrounding A. The contours are in all cases spaced by 10% of the peak emission, but start in some cases at the 5% level. The 1.1mm and 800  $\mu\text{m}$ -maps are high resolution DBMEM maps without smoothing. The 850  $\mu\text{m}$  and 450  $\mu\text{m}$ -SCUBA maps are uncalibrated and adjusted in position to agree with the UKT14-maps. The sub-mm sources are labelled in the 850  $\mu\text{m}$ -map and the HII region is marked by a 20'' circle in all maps. As in Fig. 1 the H<sub>2</sub>O maser is marked by a triangle, IRS3, the 10  $\mu\text{m}$ -source by a star, and the faint HII region G351.24+0.65 by a square. Note that the 800  $\mu\text{m}$  map does not cover the same area as the 1.1mm map. There are no data from  $\sim 50''$  north-east of A. The hole in the 850  $\mu\text{m}$  SCUBA map is due to a noisy bolometer, which was blanked out in the reduction stage.

The 800  $\mu\text{m}$ -map also shows the ridge towards the east, with the two distinct sources, MM3 and MM4, as well as the southern loop. The latter is even more prominent in the 800  $\mu\text{m}$ -map than at 1.1 mm. The western ridge is less prominent at 800  $\mu\text{m}$  and a dust condensation at  $\sim 50''$  west of A is not seen at all in the 800  $\mu\text{m}$ -map. Both maps clearly show the dust ridge to the east, which terminates in MM3.

The 2 mm-map (Fig. 1c), which has more limited spatial coverage and resolution than the other two maps, is clearly peaked on A. It does not resolve the dust emission associated with it, but about half of the flux towards NGC 6334A is due to dust emission from MM1 and MM2, the rest is free-free emission from the HII-region. The eastern source, MM3, stands out clearly, even at 2 mm, as well as the beginning of the north-eastern ridge. MM4 is only partially covered by the map, but appears to be detected at 2 mm.

### 3.2. Deduced flux densities

Since we have obtained calibrated maps at 3 wavelengths, we can use the maps to estimate the flux densities for the sources that we have identified from the maps. These integrated fluxes are given in Table 3. From the 2 mm-map we can only give the total flux of the sources closely associated with A, i.e. MM1, and MM2, because the sources are unresolved in the 2 mm beam (HPBW  $\sim 27''$ ). The eastern source, MM3, is however clearly seen in the map and MM4 may also be present. One can clearly see part of the north-eastern ridge, although the 2mm map extends only  $\sim 50''$  north-east of A, similar to the 800  $\mu\text{m}$ -map.

At 1.1mm and 800  $\mu\text{m}$  we can separate MM2 reasonably well from MM1, but we do not have enough resolution to separate MM1a and MM1b or even judge whether they are really physically separate sources. MM1a is an elongated source, which is brighter on the eastern side at long wavelengths, but

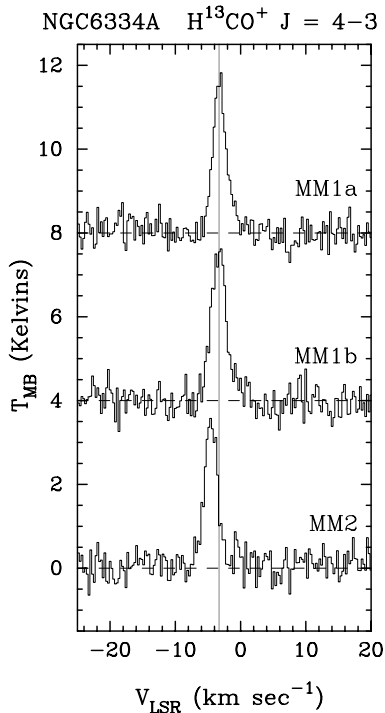


**Fig. 3.**  $\text{H}^{13}\text{CO}^+$   $J = 4-3$  spectra towards MM1a, MM1b and MM2. The horizontal line marks the velocity of NGC 6334A at a  $V_{\text{LSR}} = -3.3 \text{ km s}^{-1}$ .

shifts gradually in position towards MM1b at shorter wavelengths. At  $450 \mu\text{m}$ , MM1a is clearly arc-like, blending into MM1b in the west. At this resolution, MM1b, appears almost point like, which is why we try to separate the source into an a and a b component. This identification is, however, weak, and it is quite possible that MM1a and MM1b are part of the same source – a dust disk or torus surrounding the HII-region.

In Table 3 we also give integrated flux densities for the southern loop, i.e. the dust shell that appears to surround the southern, red-shifted free-free lobe. The integrated emission from the loop is called the dust shell in Table 3.

## 4. Discussion

### 4.1. A collimating disk around NGC 6334A

Fig. 2 present the central portion of the 1.1 mm and  $800 \mu\text{m}$  UKT14 images, as well as the  $850 \mu\text{m}$  and  $450 \mu\text{m}$  SCUBA maps. The HII-region is plotted as a  $20''$  circle on each map. One can clearly see that the dust emission appears elongated across the HII-region approximately across the waist of the HII region, with an apparent maximum on each side (MM1a & MM1b). In the south-west MM1b blends into a second source, MM2, which is located outside the HII shell and close, but not coincident with the  $20 \mu\text{m}$  source IRS3 (Harvey & Gatley 1982), also labelled IRS20 in the near-IR (Harvey et al. 1987). If the HII region is surrounded by a dust disk or torus seen approximately edge on, then one would expect to see a double peaked source. The two peaks are separated by  $\sim 10.5''$  at 1.1 mm and

**Table 3.** Integrated fluxes deduced from calibrated maps

SOURCE	2mm	1.1mm	$800 \mu\text{m}$
MM1 & 2	$15.5 \pm 2^{\text{a}}$	$18 \pm 2$	$43 \pm 8$
MM2		$9.8 \pm 2$	$18.9 \pm 5$
MM3	$1.6 \pm 0.2$	$12.1 \pm 2$	$30 \pm 5$
MM4	$0.1 \pm 0.05$	$2.0 \pm 0.5$	$4.4 \pm 0.6$
Dust shell		$5.5 \pm 2.0$	$22.0 \pm 5.0$

<sup>a</sup> The 2mm flux cannot be partitioned between MM1 & MM2. The flux quoted here is the total flux for both sources. Note that the free-free contribution from the HII region is substantial, almost half of the flux is due to free-free emission.

$\sim 12''$  and  $800 \mu\text{m}$  i.e. somewhat less than the diameter of the HII region. At  $450 \mu\text{m}$  MM1a appears like a curved arc, and MM1b has shifted even further to the west, strongly suggesting that MM1a is the dust disk surrounding the HII region, and that MM1b blends in with the disk at longer wavelengths.

What are then the properties of this disk? The total extent of the disk is  $\sim 30''$  with an aspect ratio of at least 3:1, i.e. corresponding to a linear size of  $\sim 0.2 \text{ pc}$ . The spectral energy distribution of MM1a,b and MM2 is rather shallow and similar for both source complexes. At 1.1mm we estimate the contribution from free-free emission to be  $\sim 5.5 \pm 0.5 \text{ Jy}$ . If we subtract this flux from MM1 and make isothermal fits to MM1 and MM2 (which should not be associated with free-free emission), we derive a dust emissivity index ( $\beta$ ) of  $\sim 0.7$  for both sources. Most ultracompact HII regions have  $\beta \sim 1.3-1.5$  (can be derived from data given in Sandell (1994), who presents accurate photometry on several UCHII regions). The dust in the vicinity of A is therefore distinctly different. However, the  $\beta$ -index is quite similar to what one generally finds for T Tauri stars and embedded bipolar outflow sources, which often are believed to be associated with dust disks (Weintraub, Sandell, & Duncan 1989, Woody et al. 1989, Beckwith & Sargent 1991, Chandler 1988). If we assume that the dust has a temperature of 50 K (Harvey & Gatley 1984) and take the standard Hildebrand dust opacity (Hildebrand 1983), we obtain a total mass for the disk of  $60 M_{\odot}$  and a luminosity of  $\sim 10^4 L_{\odot}$ . If the true  $\beta$ -index was higher, which it could be if there are temperature gradients over the disk, then the mass would be even higher. A hotter disk would somewhat reduce the mass. It appears plausible that such a massive disk or torus surrounding the HII region would be sufficient to collimate the outflow. Without kinematical information it is still too early to claim with certainty that MM1a is really a disk and that MM1b is a completely unrelated source (especially since they have similar radial velocities), but morphologically MM1 certainly has the appearance of a disk, even if MM1b were to be a protostellar source. Since the angular size of this disk is rather large, one should be able to easily map it with an interferometer. Even though we did not find any clear evidence for rotation in our  $\text{H}^{13}\text{CO}^+$  spectra, observations with higher spatial resolution are likely to show that this is a rotating disk.

#### 4.2. Protostellar sources

Harvey et al. (1987) proposed that IRS20 or IRS3 in the nomenclature of Harvey & Gatley (1984), is a protostar. It is very luminous ( $L \sim 10^5 L_{\odot}$ ), but it is not detected in the free-free, supporting the claim that IRS20 is a young massive star. It agrees roughly in position with the strong continuum source we call MM2, although the difference in position,  $\sim 6''$  is larger than we would expect from the positional uncertainty of our observations. Nevertheless, the strong dust emission proves that IRS20/MM2 must be surrounded by several hundred magnitudes of visual extinction. Since the star is already visible in the near- and mid-IR, it suggests that it already has shed some of its surrounding dust cocoon allowing radiation to escape from the dust core. It may therefore be more evolved than some of the other dust sources we identify in our continuum maps. Isothermal fits result in a  $\beta$ -index of  $\sim 0.8$ , which is rather uncertain, because it is based on two spectral points with rather large uncertainty due to the proximity of contaminating strong dust emission, especially from MM1b. Assuming a dust temperature of 50 K results in a total mass is  $\sim 50 M_{\odot}$  and a FIR luminosity comparable to that of MM1.

Neither MM3 and MM4 are seen in the near-IR or radio continuum, yet MM3 is rather prominent at (sub)mm wavelengths and seen clearly even at 2 mm. Neither of them are detected in the mid-IR or FIR. MM3 is surrounded by strong dust emission (Fig. 2), which is likely to raise the mass estimate of the protostar, because we will include a component of the surrounding cloud as well. The apparent dust emissivity is similar for both sources (although better constrained for MM3, where we have a clear 2 mm detection), resulting in  $\beta \sim 1.5$ – $1.6$ . If we assume that they are both self-luminous objects with dust temperatures of  $\sim 50$  K, we derive a mass of  $\sim 135 M_{\odot}$  for MM3. If the dust temperature was as low as 30 K, the mass could be as high as  $300 M_{\odot}$  for the extended dust emission associated with MM3. For MM4 the same assumptions result in a mass of  $\sim 20 M_{\odot}$ . Both these sources are ideal candidates for intermediate to high mass protostars, and well worth further studies.

#### 4.3. The dust shell surrounding the free-free outflow

Both the 1.1mm and the 800  $\mu\text{m}$  maps show a clear loop emission southwest of the HII region. This loop of emission appears to surround the redshifted free-free lobe (Fig. 1d), and it is therefore logical to assume that what we see a shell of dust which has been compressed by the free-free outflow. We also note that there is much more dust on the eastern and south-eastern side of the HII region. The red outflow therefore appears to bend to the southwest, as seen both in the ionized gas and the surrounding dust loop, i.e. in the direction where there is presumably less

resistance from the surrounding molecular cloud. To the north the cloud is more diffuse and the free-free outflow can proceed more freely. We see no dust emission associated with the northern lobe, and the direction of the flow is roughly orthogonal to the disk or torus outlined by the strong continuum source MM1.

In Table 3 we give the integrated fluxes at 1.1 mm and 800  $\mu\text{m}$  for the dust shell, but note that these fluxes have rather high errors because the emission is quite faint, especially at 1.1 mm. Nevertheless, the SED appears rather steep. We therefore assume a dust emissivity of 2, suggesting that the dust has been exposed to strong UV and shock radiation that destroys the grain mantles resulting in the more classical dust-emissivity measured for “normal” interstellar dust. Since there are no FIR observations of the dust shell, there is no way to estimate the dust temperature, but we assume that the dust will be hotter, and compute a mass for the shell assuming a dust temperature of 100 K. With these assumptions we derive a total mass for the shell of  $\sim 60 \pm 15 M_{\odot}$ .

*Acknowledgements.* I want to thank Dr Chris De Pree for helpful discussions, and Dr Luis Rodrigues for reprocessing his VLA map, so that I could overlay it on my continuum data.

#### References

- Beckwith S.V.W., Sargent A.I., 1991 ApJ 381, 250  
 Chandler C.J., 1997, In: Woodward C.E., Shull J.M., Thronson H.A. (eds.) ORIGINS. ASP Conference Series Vol. 148, Provo: Pub. ASP, p. 237  
 De Pree C.G., Goss W.M., Palmer P., Rubin R.H., 1994, ApJ 428, 670  
 De Pree C.G., Rodríguez L.F., Dickel H.R., Goss W.M., 1995, ApJ 447, 220  
 Duncan W.D., Robson E.I., Ade P.A.R., Griffin M.J., Sandell G., 1990, MNRAS 243, 126  
 Haslam C.G.T., 1974, A&AS 15, 333  
 Harvey P.M., Gatley I., 1983, ApJ 269, 613  
 Harvey P.M., Hyland A.R., Straw S.M., 1987, ApJ 317, 173  
 Hildebrand R.H., 1983, Quart.J.R.A.S. 24, 267  
 Holland W.S., Gear W.K., Lightfoot J.F., et al., 1998, In: Phillips T.G. (ed.) Advanced Technology MMW, Radio and Terahertz Telescopes. Proc SPIE vol. 3357, SPIE, Bellingham, p. 305  
 Lizano S., Heiles C., Rodríguez L.F., et al., 1988, ApJ 328, 763  
 McBreen B., Fazio G.G., Stier M., Wright E.L., 1979, ApJ 232, L183  
 Moran J.M., Rodríguez L.F., 1980, ApJ 236, L159  
 Mundt R., Brugel E.W., Bührke T., 1987, ApJ 319, 275  
 Richer J.S., 1992, MNRAS 254, 165  
 Rodríguez L.F., Cantó J., Moran J.M., 1982, ApJ 255, 103  
 Rodríguez L.F., Cantó J., Moran J.M., 1988, ApJ 333, 801  
 Rodríguez L.F., Garay G., Curiel S., et al., 1994, ApJ 430, L65  
 Sandell G., 1994, MNRAS 271, 75  
 Weintraub D.A., Sandell G., Duncan W.D., 1989, ApJ 340, L69